Ore Geology Reviews 88 (2017) 336–351

Contents lists available at ScienceDirect

Ore Geology Reviews

journal homepage: www.elsevier.com/locate/oregeo

Geostatistical modeling of the geological uncertainty in an iron ore deposit

Nadia Mery [a,b], Xavier Emery [a,b,*], Alejandro Cáceres [a,b], Diniz Ribeiro [c], Evandro Cunha [c]

[a] Department of Mining Engineering, University of Chile, Santiago, Chile
[b] Advanced Mining Technology Center, University of Chile, Santiago, Chile
[c] Gerência de Recursos Minerais Ferrosos, VALE, Belo Horizonte, Brazil

ARTICLE INFO

Article history:
Received 5 April 2017
Received in revised form 10 May 2017
Accepted 14 May 2017
Available online 18 May 2017

Keywords:
Geological heterogeneity
Geological control
Geological domaining
Geostatistical simulation
Stoichiometric closure

ABSTRACT

This paper addresses the problem of quantifying the joint uncertainty in the grades of elements of interest (iron, silica, manganese, phosphorus and alumina), loss on ignition, granulometry and rock types in an iron ore deposit. Sampling information is available from a set of exploration drill holes. The methodology considers the construction of multiple rock type outcomes by plurigaussian simulation, then outcomes of the quantitative variables (grades, loss on ignition and granulometry) are constructed by multigaussian joint simulation, accounting for geological domains specific to each quantitative variable as well as for a stoichiometric closure formula linking these variables. The outcomes are validated by checking the reproduction of the data distributions and of the data values at the drill hole locations, and their ability to measure the uncertainty at unsampled locations is assessed by leave-one-out cross validation.

Both the plurigaussian and multigaussian models offer much flexibility to the practitioner to face up to the complexity of the variables being modeled, in particular: (1) the contact relationships between rock types, (2) the geological controls exerted by the rock types over the quantitative variables, and (3) the cross-correlations and stoichiometric closure linking the quantitative variables. In addition to this flexibility, the use of efficient simulation algorithms turns out to be essential for a successful application, due to the high number of variables, data and locations targeted for simulation.

1. Introduction

This work presents an application of geostatistical simulation for assessing the mineral resources and quantifying the geological uncertainty in an iron ore deposit. Although it uses well-known models (plurigaussian and multigaussian), it is innovative for several reasons. The first one is the high dimensionality of the problem under consideration, which involves one nominal variable with ten categories (rock types) and seven quantitative variables (grades of five elements of interest, loss on ignition and granulometry). The second innovation relates to the different geological controls exerted by the rock types over the quantitative variables, which implies the definition of geological domains proper to each quantitative variable and the fact that one variable may be continuous across a rock type boundary, while other variables may be discontinuous when crossing the same boundary. The third distinctive feature is that all the quantitative variables are assumed to be cross-correlated, even when they are defined in disjoint or partially overlapping geological domains, so that the presence of a rock type boundary does not screen out the influence of the data between both sides of the boundary. The last innovation corresponds to the generation of simulated outcomes (scenarios) that reproduce a stoichiometric closure formula between the grades and the loss on ignition.

The proposed approach is hierarchical, in which one first simulates the rock types, then the remaining variables conditionally to the rock types, a strategy that is commonly used when modeling mineral resources (e.g., Roldão et al., 2012; Jones et al., 2013; Talebi et al., 2016). The outline of the next sections is the following: after presenting the case study (Section 2), we address the modeling and simulation of the rock types (Section 3), then the modeling and joint simulation of the quantitative variables (grades, loss on ignition and granulometry) (Section 4). A general discussion and conclusions follow.

* Corresponding author at: Department of Mining Engineering, University of Chile, Santiago, Chile.
E-mail addresses: nmery@ing.uchile.cl (N. Mery), xemery@ing.uchile.cl (X. Emery), alecacer@gmail.com (A. Cáceres), diniz.ribeiro@vale.com (D. Ribeiro), evandro.cunha@vale.com (E. Cunha).

http://dx.doi.org/10.1016/j.oregeorev.2017.05.011
0169-1368/

2. Presentation of the deposit and the data

The ore deposit under study is located in the Minas Gerais State, Brazil, and is hosted in banded iron formations. Its dimensions are about 2000 meters along the east–west direction, 1000 meters along the north–south and 500 meters along the vertical. The main iron-bearing minerals are hematite ores (high-grade) and itabirites (low-grade), which can be found either as dense (compact) or porous (friable) rocks. The transition from high-grade to low-grade iron minerals is mainly characterized by an increase of the quartz content. Also, the deposit is overlaid by a supergene layer (known as surficial canga), formed with iron-rich fragments and itabirites cemented with goethite derived from the weathering of iron formation (Dorr, 1964).

An exploration campaign consisting of diamond drill holes has been realized to recognize the deposit and to quantify its resources. The sampling design has a horizontal spacing varying from 50 m × 50 m to 100 m × 100 m (Fig. 1). Along the drill holes, 4465 data have been obtained at a composite length of 10 meters (with a minimum length of 3 meters), with information on the grades of five elements of interest (iron, silica, phosphorus, alumina and manganese), loss on ignition, granulometry above 6.3 mm, and prevailing rock type (Tables 1 and 2). The two main rock groups, hematite ores and itabirites, are subdivided depending on their contents in iron (iron-rich hematite vs. iron-poor itabirite), silica, alumina, manganese, loss on ignition and granulometry, whereas the waste material consists of dolomite, laterite, phyllite, intrusive rocks and barren rocks without economic interest. The experimental distributions of the grades, loss on ignition and granulometry are displayed in Fig. 2. The iron

Table 1
Quantitative variables with their codification and definition.

Variable	Unit	Symbol	Definition
Iron grade	%	Fe	Mass concentration of iron (Fe)
Silica grade	%	SiO_2	Mass concentration of silicon dioxide (SiO_2)
Phosphorus grade	%	P	Mass concentration of phosphorus (P)
Alumina grade	%	Al_2O_3	Mass concentration of aluminum oxide (Al_2O_3)
Manganese grade	%	Mn	Mass concentration of manganese (Mn)
Loss on ignition	%	LOI	Mass concentration of volatile materials (combined water, organic matter, soluble salts, carbonates, sulfides)
Granulometry	%	G_1	Mass proportion of fragments with size > 6.3 mm

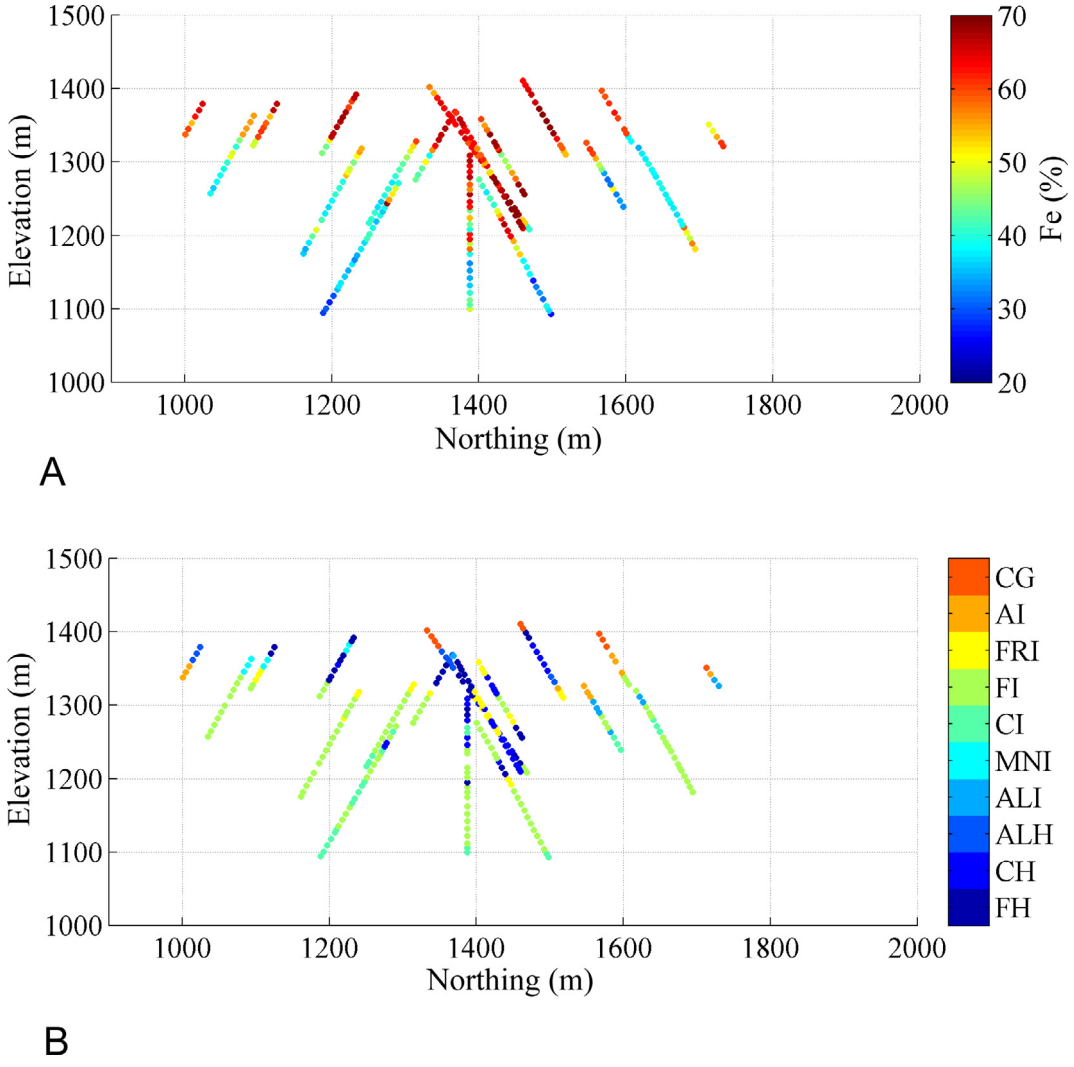

Fig. 1. Location of drill hole samples, painted according to iron grade (A) and rock type (B) (cross sections with easting coordinate comprised between −6450 m and −6350 m).

Table 2
Rock types and their codification.

Rock type	Symbol	Code
Friable hematite	FH	1
Compact hematite	CH	2
Alumina-rich hematite	ALH	3
Alumina-rich itabirite	ALI	4
Manganese-rich itabirite	MNI	5
Compact itabirite	CI	6
Friable itabirite	FI	7
Friable iron-rich itabirite	FRI	8
Amphibolitic itabirite	AI	9
Canga	CG	10
Waste	W	11

and silica grade distributions are bimodal, suggesting the mixing of more than one population of data, while the other distributions are unimodal and positively skewed. One also notices the strong influence of the rock type on the grade, loss on ignition and granulometry distributions, in particular, in their spreads and mean values (Table 3), which agrees with the rock type definition. Finally, Fig. 1 also suggests the presence of trends that are controlled by the rock type; in particular, high iron grades are mostly found at higher elevations, which correspond to hematite ores and canga. Likewise, high values of granulometry are expected to be found at lower elevations, corresponding to compact itabirite. In summary, the rock type exerts a control over the statistical and spatial behavior of the quantitative variables of interest (grades, loss on ignition and granulometry). These statements motivate the recourse to a hierarchical approach, where the rock type is modeled prior to the quantitative variables.

3. Rock type modeling and simulation

Based on the drill hole data and the understanding of the deposit, the spatial layout of the rock type domains has been modeled by the resource geologists on a regular grid containing $219 \times 108 \times 55$ nodes with spacing $10\,\text{m} \times 10\,\text{m} \times 10\,\text{m}$ (Fig. 3). However, this model corresponds to a single interpretation of the deposit and does not allow quantifying the uncertainty in the true rock type layout. For this reason, it is of interest to construct a set of outcomes, via stochastic simulation, that provide alternative interpretations of the rock type distribution within the deposit. In the following, the plurigaussian model (Le Loc'h and Galli, 1997; Armstrong et al., 2011; Yunsel and Ersoy, 2011; Talebi et al., 2016) will be used for this purpose. For the sake of simplicity, the layout of the waste (located in the outer part of the deposit) is assumed to be perfectly known, so that the simulation will be restricted to the ten ore rock types.

3.1. Truncation rule

The plurigaussian model defines a categorical variable (in the present case, the rock type) through the truncation of synthetic Gaussian random fields. The number of such fields and the way to truncate them (truncation rule) are chosen in order to reproduce the contact relationships between the rock types, which here relate to transitions in the granulometry (fine vs. coarse), loss on ignition or grade of an element of interest (poor vs. rich).

To this end, a six-dimensional truncation rule is defined, based on six underlying Gaussian random fields, denoted in the following as $Y_1, \ldots, Y_6$. The first random field is introduced to split the ore into the canga (CG) and all the remaining ferruginous rock types (hematite ores and itabirites) (Fig 4A). The latter are then split into two groups (friable rocks and compact rocks) thanks to a second random field associated with the ore granulometry (Fig 4A, B). The third random field, associated with the iron content (or with the silica content, which is strongly negatively correlated with the iron content, see Section 4 next), allows splitting the compact group into compact hematite (CH) and compact itabirite (CI), and the friable group into iron-poor itabirite (FI), iron-rich itabirites and friable hematite ores (Fig 4B, C). In turn, the fourth random field, associated with the alumina content, is used to split the friable hematite ores into alumina-poor (FH) and alumina-rich (ALH), as well as the iron-rich itabirites into alumina-poor (FRI) and alumina-rich (Fig 4C). The fifth random field, associated with the manganese content, is introduced to split the alumina-rich itabirites into manganese-rich (MNI) and manganese-poor itabirites. The latter are finally split into amphibolitic (AI) and alumina-rich (ALI) itabirites by considering a sixth random field related with the loss on ignition (and, to some extent, with the phosphorus grade that positively correlates with the loss on ignition) (Fig 4D). Such an ordering has been chosen because it allows splitting the deposit into the ten rock types by using only six Gaussian random fields, which furthermore have a one-to-one correspondence with the canga layer, granulometry, iron, alumina, manganese and loss on ignition contents, respectively. Other orderings of the truncation rule would require more Gaussian random fields and the previous one-to-one correspondence would be lost, therefore the interpretation of the truncation rule would be less straightforward.

The proposed truncation rule also agrees with the contact relationships observed on the drill hole data (Table 4), which indicate few contacts between several pairs of rock types that are remote in the truncation rule (in particular, FI-FH, FI-CH, FI-ALH, FH-ALI, FH-MNI, FH-CI, FH-AI, ALH-CI and ALH-FRI) and many contacts between pairs that are contiguous in the truncation rule (FH-CH, FH-FRI, ALI-FI, CI-FI and FI-FRI). Other contacts that seem possible on the truncation rule (e.g., CG-CI or CG-FI) will actually be scarce or inexistent because, at each location in the deposit, one of the two rock types will be assigned a local proportion close to zero, as it will be seen in the next subsection.

3.2. Truncation thresholds

The previous truncation rule depends on nine thresholds $\{t_1, t_2, t_3, t_3', t_3'', t_4, t_4', t_5, t_6\}$ that delimit the partition of the six-dimensional space into parallelotopes (Fig. 4). Let $p_1, \ldots p_{10}$ be the proportions of the ten rock types of interest (mean values of the associated indicator variables), ordered according to the numbering of Table 2. Assuming that the underlying Gaussian random fields are independent and denoting by G the standard normal cumulative distribution function, one has the following relationships between rock type proportions and thresholds:

$$\begin{cases} p_1 = [1-G(t_1)]G(t_2)[1-G(t_3')]G(t_4') \\ p_2 = [1-G(t_1)][1-G(t_2)][1-G(t_3')] \\ p_3 = [1-G(t_1)]G(t_2)[1-G(t_3')][1-G(t_4')] \\ p_4 = [1-G(t_1)]G(t_2)[G(t_3')-G(t_3)][1-G(t_4)][1-G(t_5)]G(t_6) \\ p_5 = [1-G(t_1)]G(t_2)[G(t_3')-G(t_3)][1-G(t_4)]G(t_5) \\ p_6 = [1-G(t_1)][1-G(t_2)]G(t_3') \\ p_7 = [1-G(t_1)]G(t_2)G(t_3) \\ p_8 = [1-G(t_1)]G(t_2)[G(t_3')-G(t_3)]G(t_4) \\ p_9 = [1-G(t_1)]G(t_2)[G(t_3')-G(t_3)][1-G(t_4)][1-G(t_5)][1-G(t_6)] \\ p_{10} = G(t_1) \end{cases} \quad (1)$$

Knowing the rock type proportions, it is therefore straightforward to derive the truncation thresholds.

From a geological point of view, the rock type proportions are not homogeneous across the deposit. For instance, canga (CG) is

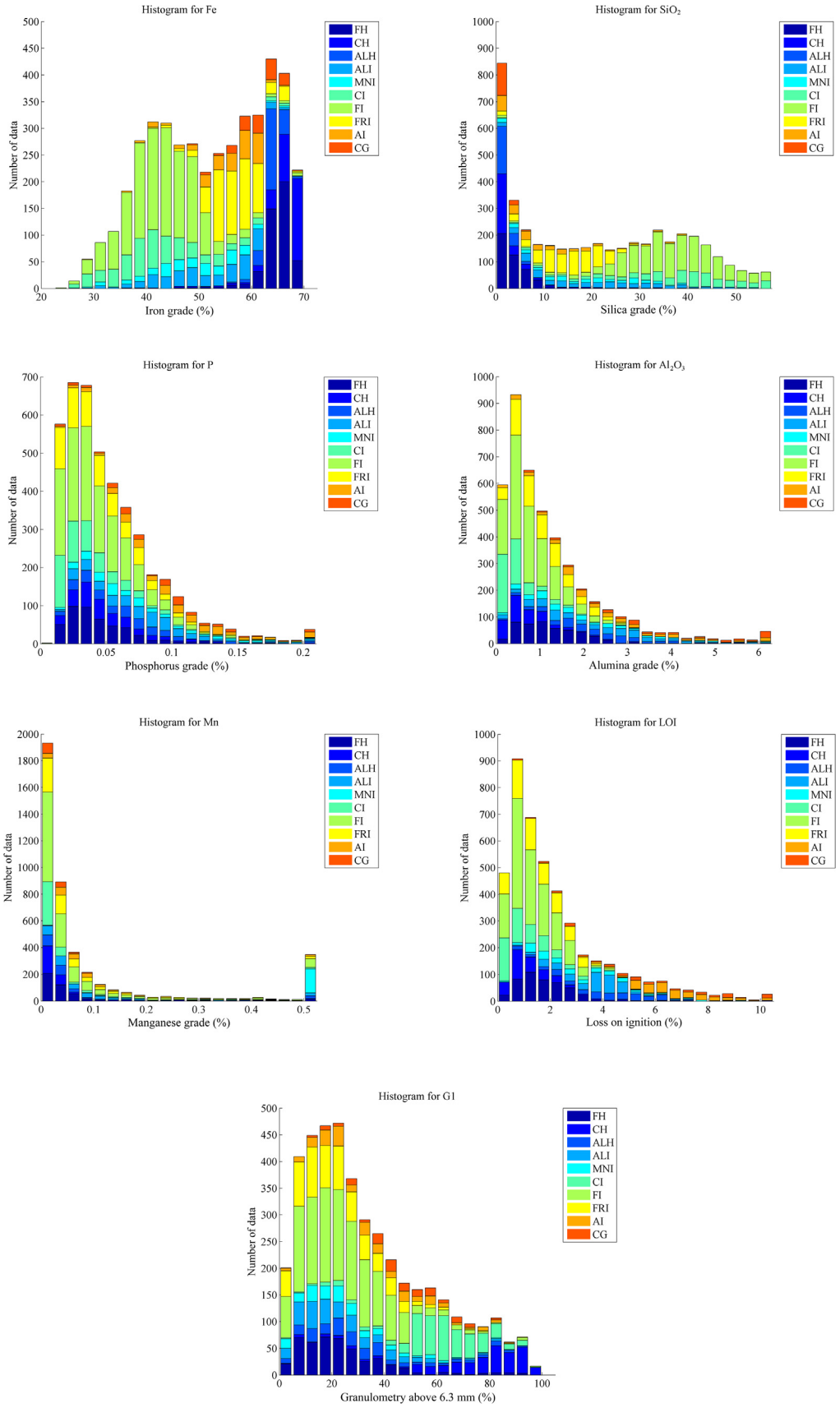

Fig. 2. Experimental distributions of quantitative variables.

Table 3
Relationships between rock types and quantitative variables (average values are indicated into parentheses). In this table, "rich" means greater than 62% for iron, 35% for silica, 1.5% for alumina, 1% for manganese, 4.5% for loss on ignition. "Poor" means less than 45% for iron, 10% for silica, 1.5% for alumina, 1% for manganese, 2% for loss on ignition. For granulometry, "fine" means less than 40%, and "coarse" more than 50%.

Rock type	Iron grade	Silica grade	Alumina grade	Manganese grade	Loss on ignition	Granulometry
FH	Rich (64.8)	Poor (4.0)	Poor (1.2)	Poor (0.13)	Poor (1.8)	Fine (23.8)
CH	Rich (66.2)	Poor (3.2)	Poor (0.7)	Poor (0.04)	Poor (1.3)	Coarse (72.2)
ALH	Rich (64.0)	Poor (1.9)	Rich (2.1)	Poor (0.23)	Intermediate (3.9)	Fine (33.4)
ALI	Intermediate (51.6)	Intermediate (20.1)	Rich (2.0)	Poor (0.13)	Intermediate (3.6)	Fine (24.4)
MNI	Intermediate (49.3)	Intermediate (20.2)	Rich (1.7)	Rich (3.24)	Intermediate (2.8)	Fine (25.0)
CI	Poor (42.7)	Rich (37.2)	Poor (0.5)	Poor (0.10)	Poor (1.1)	Coarse (60.5)
FI	Poor (42.9)	Rich (36.2)	Poor (0.8)	Poor (0.09)	Poor (1.4)	Fine (24.9)
FRI	Intermediate (57.0)	Intermediate (15.6)	Poor (1.1)	Poor (0.09)	Poor (1.5)	Fine (22.4)
AI	Intermediate (55.4)	Intermediate (11.8)	Rich (2.0)	Poor (0.13)	Rich (6.3)	Fine (36.3)
CG	Rich (63.0)	Poor (2.2)	Rich (2.6)	Poor (0.05)	Rich (4.6)	Intermediate (46.9)

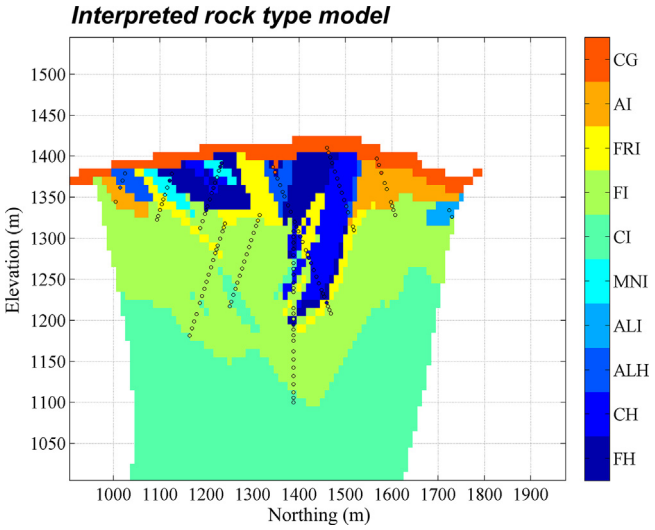

Fig. 3. A cross section of the interpreted rock type model (easting coordinate = −6400 m). White areas correspond to waste or air. The drill hole data belonging to this cross-section have been superimposed.

a surficial layer covering the deposit while the compact rock types (CH and CI) are more likely to be found in depth rather than near the surface. Lateral variations are also observed, as shown in the interpreted lithological model (Fig. 3). Following Beucher et al. (1993), the rock type proportions (hence, the truncation thresholds) will be assumed to vary in space, in order to reproduce the observed trends in the rock type proportions. To this end, for each target location, the local proportions are calculated from the interpreted lithological model by using a moving window with size 50 m × 50 m × 30 m centered on the location under consideration. The moving window size has been defined in accordance with the resources geologists and the performance of the resulting model has been checked by the split-sample validation technique (see next subsection).

3.3. Variogram analysis

For each Gaussian random field and each truncation threshold, the rock type data can be codified into indicators, valued as 0, 1 or unknown (Table 5). The experimental variograms of the indicator data so defined are then calculated along the main directions of anisotropy, i.e., the horizontal plane for lag separation distances multiple of 50 meters and the vertical direction for lag separation distances multiple of 10 meters, in both cases with an angular tolerance of 90° on the azimuth and 20° on the dip.

The indicator variograms are subsequently converted into variograms of the underlying Gaussian random fields, by using the well-known relationship between indicator and Gaussian variograms (Kyriakidis et al., 1999; Emery, 2007; Maleki et al., 2016), and finally fitted by nesting basic theoretical variogram models with a geometric anisotropy (Fig. 5 and Table 6). The fitting is realized by a semi-automated algorithm ensuring that the sill of each variogram is equal to 1 (Emery, 2010), as the Gaussian random fields are assumed to have a unit variance. Based on a visual appraisal of Fig. 5, the fit is deemed satisfactory for all the Gaussian random fields, since the fitted variogram models pass close to the calculated experimental points along both the horizontal and vertical directions.

The previous approach for variogram analysis remains applicable even if the indicator data exhibit different directions of anisotropy (i.e., if the main directions of continuity of the rock type domains are not the same), in which case the variogram models fitted to the Gaussian random fields would also have different directions of anisotropy. Also note that the cross-variograms of the Gaussian random fields are identically zero functions, since these fields are assumed independent. Although this assumption limits the generality of our plurigaussian model (no fit of the indicator cross-variograms is undertaken), it allows inferring the truncation thresholds and the variograms of the Gaussian random fields in a hierarchical manner, whereas a joint inference procedure would have to be designed if these fields were not independent.

3.4. Simulation

The simulation is performed in three steps:

(1) The six underlying Gaussian random fields $Y_1, \ldots, Y_6$ are first simulated at the data locations, conditionally to the indicator data (Table 5), by resorting to an iterative algorithm (Gibbs sampler) (Freulon, 1994; Armstrong et al., 2011). To improve the convergence of the simulated values to the target multivariate Gaussian distribution, a unique neighborhood implementation is used (Emery et al., 2014). The sampler is stopped when each Gaussian data has been updated one hundred times.
(2) The Gaussian random fields are then simulated at the target locations, conditionally to the Gaussian data produced by the Gibbs sampler. Non-conditional outcomes of each Gaussian random field are constructed with a spectral turning-bands algorithm (Emery et al., 2016) and converted into conditional outcomes by residual kriging (Chilès and Delfiner, 2012).
(3) The simulated Gaussian random fields are finally truncated in order to obtain the rock type domains, according to the previously defined truncation rule (Fig. 4).

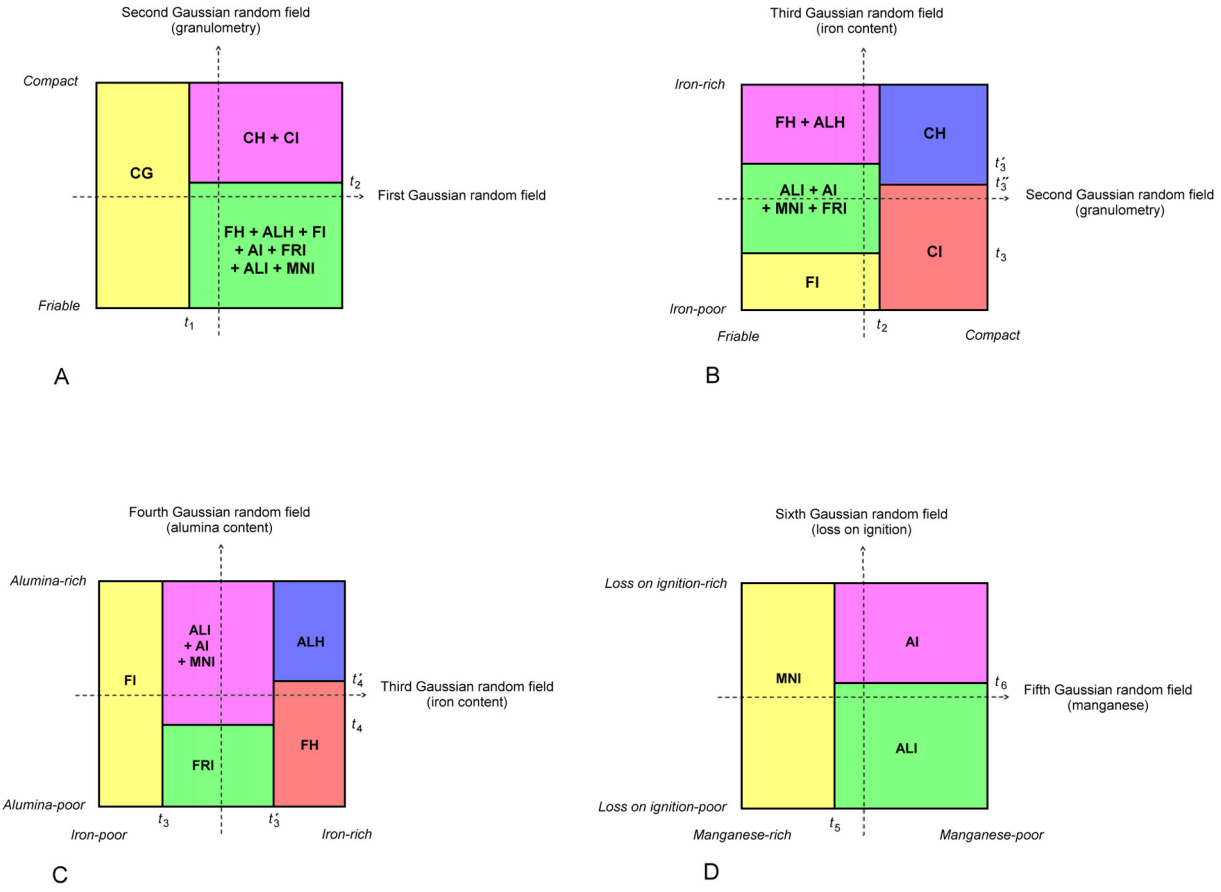

Fig. 4. Representations of the truncation rule along dimensions 1 & 2 (A), dimensions 2 & 3 (B), dimensions 3 & 4 (C) and dimensions 5 & 6 (D).

Table 4
Number of rock type transitions, considering pairs of adjacent data along each drill hole.

		Rock type of the top data									
		FH	**CH**	**ALH**	**ALI**	**MNI**	**CI**	**FI**	**FRI**	**AI**	**CG**
Rock type of the bottom data	**FH**	227	37	31	11	6	4	8	26	5	31
	CH	33	162	6	3	0	15	16	21	1	5
	ALH	22	12	123	4	2	1	1	4	14	14
	ALI	15	9	7	142	9	5	37	31	36	7
	MNI	15	0	6	11	105	3	22	16	0	3
	CI	3	11	1	19	7	231	135	24	3	0
	FI	31	21	2	57	23	92	758	107	15	0
	FRI	74	22	17	21	15	14	34	304	10	11
	AI	3	0	20	20	1	0	15	6	127	17
	CG	1	0	2	0	0	0	0	0	0	51

Table 5
Codification of rock type data into indicator data.

Rock type	$Y_1 < t_1$	$Y_2 < t_2$	$Y_3 < t_3$	$Y_3 < t'_3$	$Y_3 < t''_3$	$Y_4 < t_4$	$Y_4 < t'_4$	$Y_5 < t_5$	$Y_6 < t_6$
FH	0	1	0	0	–	–	1	–	–
CH	0	0	–	–	0	–	–	–	–
ALH	0	1	0	0	–	–	0	–	–
ALI	0	1	0	1	–	0	–	0	1
MNI	0	1	0	1	–	0	–	1	–
CI	0	0	–	–	1	–	–	–	–
FI	0	1	1	1	–	–	–	–	–
FRI	0	1	0	1	–	1	–	–	–
AI	0	1	0	1	–	0	–	0	0
CG	1	–	–	–	–	–	–	–	–

Twenty outcomes are constructed on the same grid as the interpreted rock type model, by changing in each outcome the seeds for generating random numbers in the Gibbs sampler and the spectral turning-bands algorithm. A few outcomes are mapped in Fig. 6.

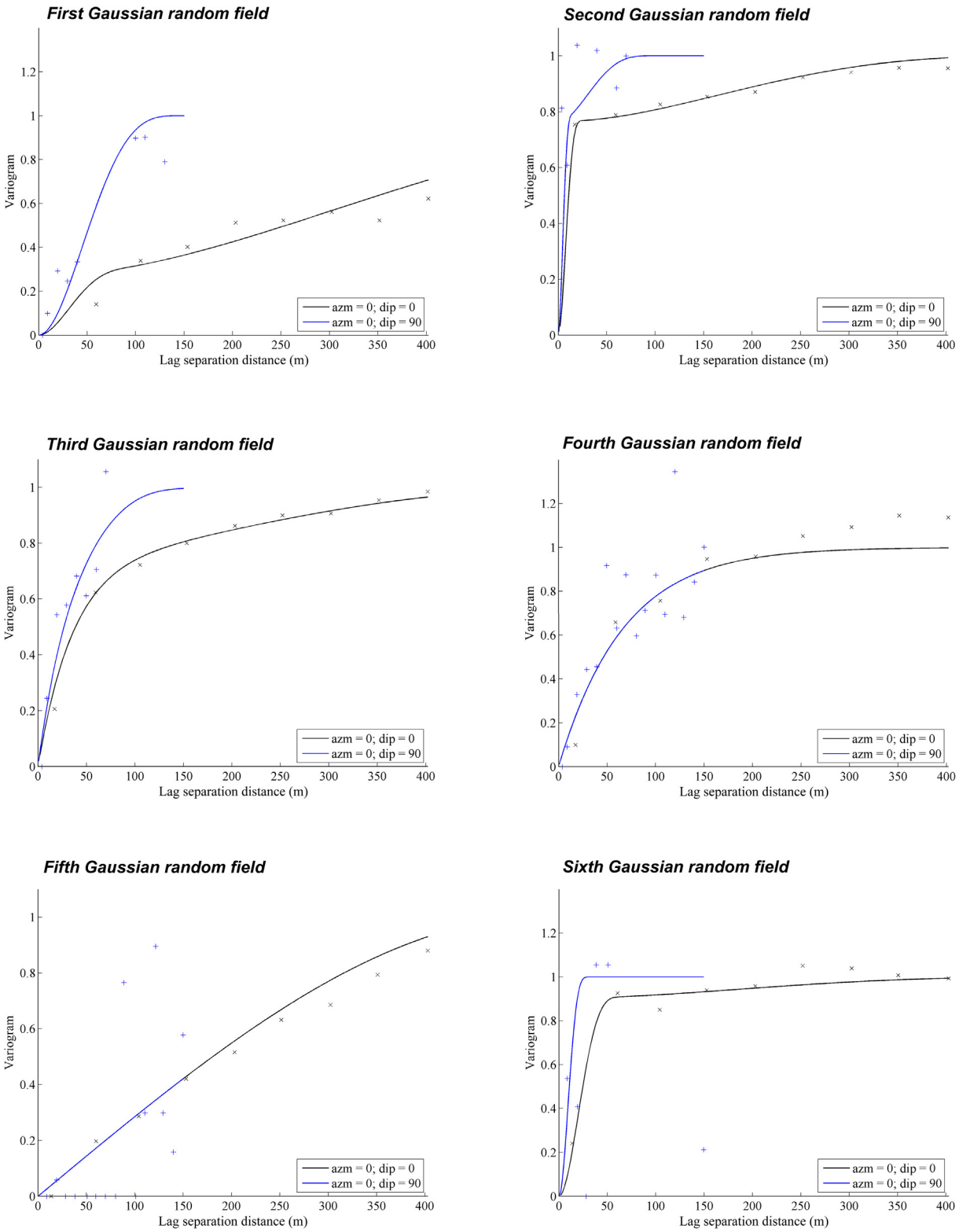

Fig. 5. Experimental (crosses) and fitted (solid lines) variograms of the underlying Gaussian random fields, along the main anisotropy directions: horizontal (black) and vertical (blue). (For interpretation of the references to colour in this figure legend, the reader is referred to the web version of this article.)

3.5. Split-sample validation

The original drill hole data are divided into two subsets (a training subset and a testing subset, each with approximately 50% of the data) by a random selection and the data of the training subset are used as conditioning information for simulating the rock types at the locations of the testing subset. With the outcomes so obtained, the probability of occurrence of each rock type can be calculated at the testing subset locations. Among the locations with a given probability p of occurrence of a rock type, one expects that a proportion p of the testing data actually match this rock type, which provides a simple way of validating the accuracy of the

Table 6
Parameters of the fitted variograms.

Gaussian random field	Basic nested structure	Horizontal range (m)	Vertical range (m)	Sill
1	Cubic	100	150	0.271
	Cubic	1000	150	0.729
2	Cubic	25	15	0.765
	Cubic	550	100	0.235
3	Exponential	110	85	0.761
	Cubic	700	165	0.239
4	Exponential	200	200	1.000
5	Spherical	520	520	1.000
6	Cubic	65	30	0.903
	Cubic	600	35	0.097

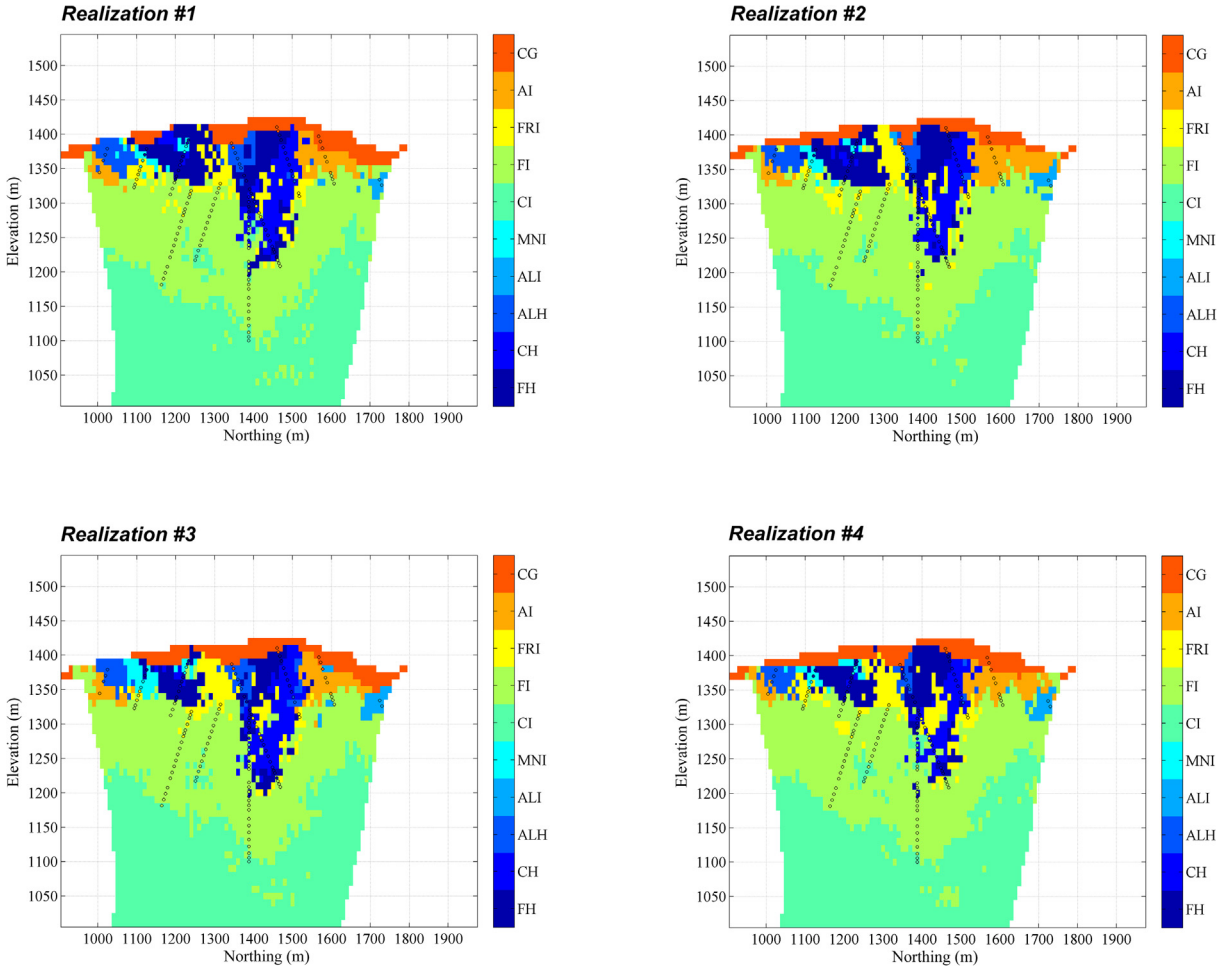

Fig. 6. Cross section of four rock type outcomes (easting = −6400 m). The conditioning drill hole data belonging to this cross-section have been superimposed.

model (Deutsch, 1997; Goovaerts, 2001). The comparison between probabilities of occurrence and proportions of testing data is realized for the different rock types and different probabilities (0.1, 0.3, 0.5, 0.7 and 0.9, each with a calculation tolerance of ±0.1), yielding an excellent match in all the cases (Fig. 7).

4. Modeling and simulation of quantitative variables

4.1. Need for joint simulation

Having simulated the rock type layout within the deposit, we now tackle the problem of simulating the quantitative variables (grades, loss on ignition and granulometry). Two reasons justify the need for a joint simulation rather than a simulation of each variable separately. The first one is the existence of strong cross-correlations between several pairs of variables, such as Fe-SiO_2, LOI-P and LOI-Al_2O_3 over the whole dataset (Table 7). Significant correlations can also be observed within specific rock types, for instance, −0.80 and −0.73 for the pairs Fe-Al_2O_3 and Fe-LOI in canga, respectively.

The second reason is the stoichiometric closure formula linking the grade variables and loss on ignition, which therefore constitute a regionalized composition:

$$1.4297\mathrm{Fe} + \mathrm{SiO_2} + \mathrm{Al_2O_3} + 2.2913\mathrm{P} + 1.2912\mathrm{Mn} + \mathrm{LOI} = 100. \quad (2)$$

The coefficients 1.4297, 2.2913 and 1.2912 are introduced to rescale the masses of iron, phosphorus and manganese to the

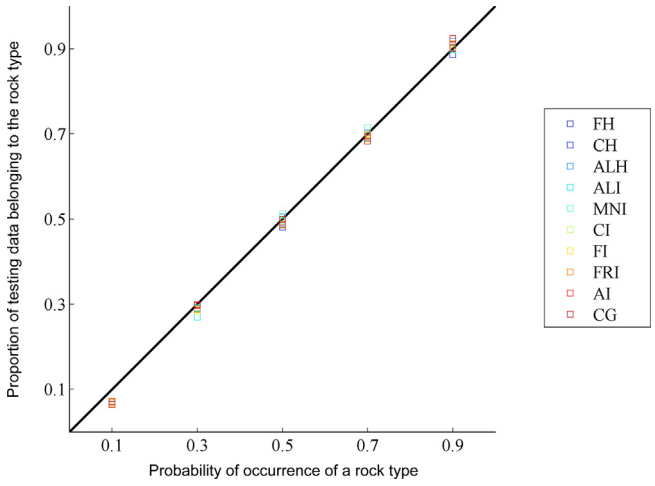

Fig. 7. Results of split-sample validation of plurigaussian simulation.

masses of the oxides bearing these elements: hematite (Fe_2O_3), phosphorus pentoxide (P_2O_5) and manganese monoxide (MnO), respectively. To reproduce this closure formula, the following change of variables is proposed, in which the quantitative variables (ordered from the variable with the lowest mean value to the variable with the greatest mean value) are successively normalized by the residual of the stoichiometric closure:

$$\begin{cases} Z_1 = \mathrm{P} \\ Z_2 = \frac{1.2912\mathrm{Mn}}{100-2.2913\mathrm{P}} \\ Z_3 = \frac{\mathrm{Al_2O_3}}{100-2.2913\mathrm{P}-1.2912\mathrm{Mn}} \\ Z_4 = \frac{\mathrm{LOI}}{100-2.2913\mathrm{P}-1.2912\mathrm{Mn}-\mathrm{Al_2O_3}} \\ Z_5 = \frac{\mathrm{SiO_2}}{100-2.2913\mathrm{P}-1.2912\mathrm{Mn}-\mathrm{Al_2O_3}-\mathrm{LOI}} \\ Z_6 = \mathrm{G_1} \end{cases} \quad (3)$$

One therefore has to address the joint simulation of the six variables Z_1 to Z_6, which allow recovering the seven original variables, as per the following back-transformation:

$$\begin{cases} \mathrm{P} = Z_1 \\ \mathrm{Mn} = \frac{Z_2(100-2.2913\mathrm{P})}{1.2912} \\ \mathrm{Al_2O_3} = Z_3(100-2.2913\mathrm{P}-1.2912\mathrm{Mn}) \\ \mathrm{LOI} = Z_4(100-2.2913\mathrm{P}-1.2912\mathrm{Mn}-\mathrm{Al_2O_3}) \\ \mathrm{SiO_2} = Z_5(100-2.2913\mathrm{P}-1.2912\mathrm{Mn}-\mathrm{Al_2O_3}-\mathrm{LOI}) \\ \mathrm{Fe} = \frac{100-2.2913\mathrm{P}-1.2912\mathrm{Mn}-\mathrm{Al_2O_3}-\mathrm{LOI}-\mathrm{SiO_2}}{1.4297} \\ \mathrm{G_1} = Z_6 \end{cases} \quad (4)$$

Since the mean values of P, Mn, Al_2O_3 and LOI are much smaller than 100, the new variables Z_2 to Z_6 turn out to be strongly correlated (correlation coefficients greater than 0.995) with the variables appearing in the numerators, i.e., Mn, Al_2O_3, LOI and SiO_2, respectively (Table 8). Put in other words, the transformation has been chosen in order to produce the smallest distortion between the original quantitative variables and the new transformed variables. Also note that the latter are not additive, i.e., they do not average linearly onto a support greater than the data support (quasi-point support), since they are defined as ratios of grades. Accordingly, simulation will be performed on a point support; any change of support would require to consider a fine grid and to average the simulated original (back-transformed) variables obtained on this fine grid onto the blocks of interest.

4.2. Geological domaining

The rock types control the statistical behavior of both the original and new variables. It is therefore appropriate to partition the deposit into rock type domains in which the variables can be assumed to be homogeneously distributed and represented by stationary random fields (Rossi and Deutsch, 2014). One of these domains for all the variables is the canga, due to its supergene nature and superficial position. The other domains should, however, be defined differently for each variable, as explained next.

For variable Z_5, one can distinguish three domains in addition to canga: the first one is an iron-poor silica-rich itabirite formed by CI + FI; the second one is formed by the iron-rich silica-poor hematite ores (FH + CH + ALH); the third one consists of the remaining itabirites (ALI + MNI + FRI + AI) with intermediate iron and silica grades. For variables Z_1, Z_3 and Z_4 (related to the phosphorus grade, alumina grade and loss on ignition, respectively), one can distinguish a rock type domain (AI) with the highest average values and variances, a second group of rock types (FH + CH + CI + FI + FRI) with low values, and a third group (ALH + ALI + MNI) with intermediate values. For variable Z_2 (related to the manganese grade), the manganese-rich itabirite (MNI) appears to be very different from all the other rock types (Table 3) and should therefore constitute a separate domain. Finally, for variable Z_6 (related to the granulometry), the logical partitioning consists of the compact (CH + CI) versus the friable (FH + ALH + ALI + MNI + FI + FRI + AI) rock types.

A summary of the geological domains is given in Table 9. Fig. 8 shows an example of contact analysis (Rossi and Deutsch, 2014; Maleki and Emery, 2015), which consists in grouping the data of a geological domain according to their distances to the boundary with another domain and in calculating the mean value of each group. This analysis allows checking that the local mean value changes significantly when crossing the boundary between one domain and another. An analysis of the cross-correlation between domains could also be undertaken, but this is actually not critical in the present case study, insofar as we will develop a model where all the variables are cross-correlated, irrespective of whether they are defined in the same domain or not (see next subsection).

4.3. Geostatistical modeling

Each variable $Z_1 \ldots Z_6$ can be represented by a stationary random field within each of the associated geological domain, totaling 22 random fields that are defined on domains that can be the same,

Table 7
Experimental correlation matrix between quantitative variables.

	Fe	SiO_2	P	Al_2O_3	Mn	LOI	G_1
Fe	1	−0.98	0.13	0.23	−0.12	0.19	0.13
SiO_2	−0.98	1	−0.24	−0.35	−0.01	−0.34	−0.10
P	0.13	−0.24	1	0.37	0.15	0.69	0.02
Al_2O_3	0.23	−0.35	0.37	1	0.15	0.61	−0.26
Mn	−0.12	−0.01	0.15	0.15	1	0.19	−0.08
LOI	0.19	−0.34	0.69	0.61	0.19	1	−0.03
G_1	0.13	−0.10	0.02	−0.26	−0.08	−0.03	1

Table 8
Experimental correlation coefficients between original and new variables.

	Fe	SiO_2	P	Al_2O_3	Mn	LOI	G_1
Z_1	0.13	−0.26	1.00	0.42	0.15	0.71	0.03
Z_2	−0.14	−0.01	0.15	0.15	1.00	0.18	−0.07
Z_3	0.17	−0.34	0.42	1.00	0.20	0.68	−0.18
Z_4	0.17	−0.36	0.71	0.70	0.25	1.00	−0.01
Z_5	−0.98	1.00	−0.24	−0.33	0.01	−0.34	−0.11
Z_6	0.13	−0.10	0.03	−0.18	−0.07	−0.01	1.00

Table 9
Geological domains associated with each quantitative variable to simulate.

Variable	Domain 1	Domain 2	Domain 3	Domain 4
Z_1	AI	FH + CH + CI + FI + FRI	ALH + ALI + MNI	CG
Z_2	MNI	FH + CH + ALH + ALI + CI + FI + FRI + AI	CG	
Z_3	AI	FH + CH + CI + FI + FRI	ALH + ALI + MNI	CG
Z_4	AI	FH + CH + CI + FI + FRI	ALH + ALI + MNI	CG
Z_5	CI + FI	ALI + MNI + FRI + AI	FH + CH + ALH	CG
Z_6	CH + CI	FH + ALH + ALI + MNI + FI + FRI + AI	CG	

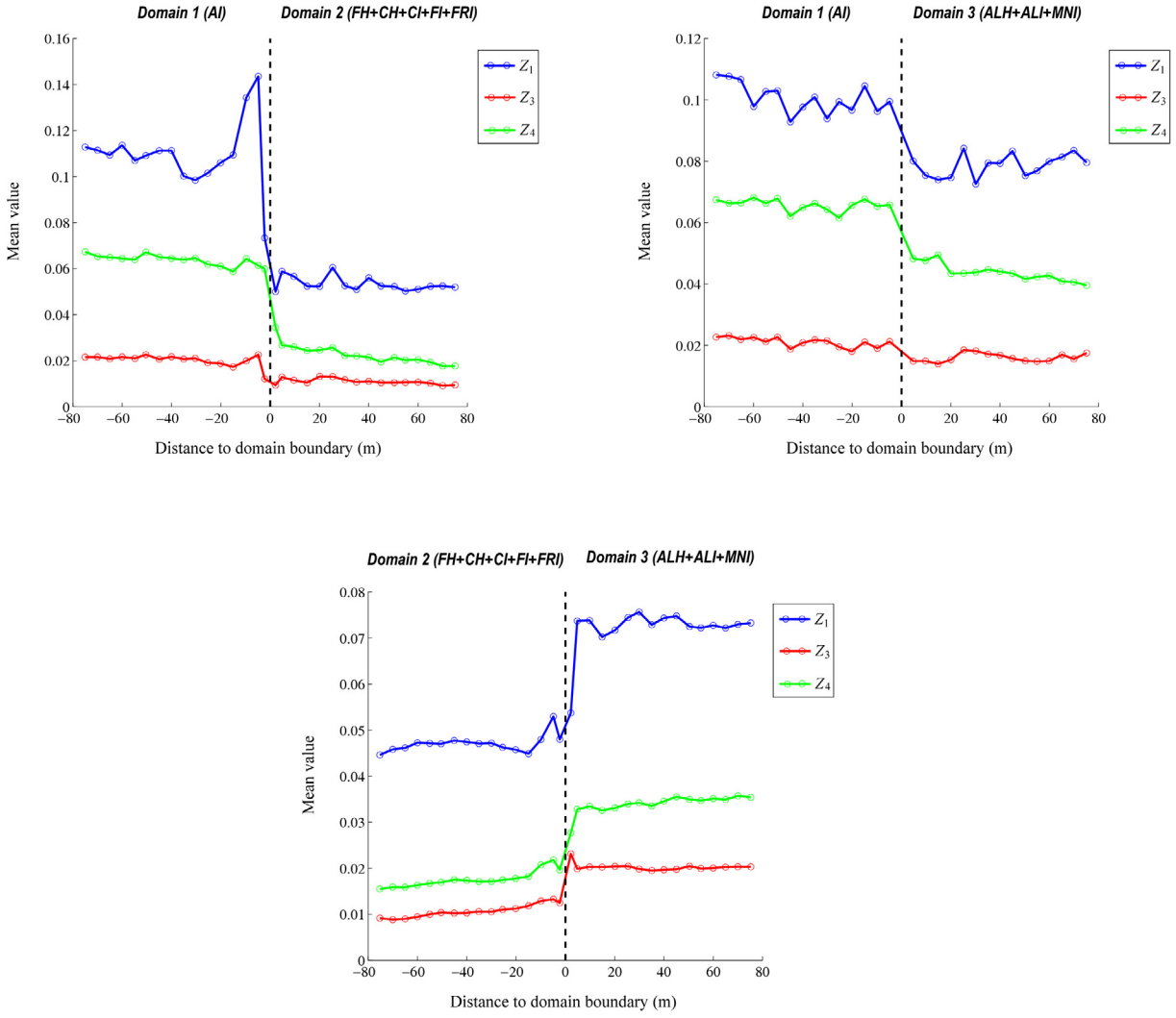

Fig. 8. Evolution of the mean values of Z_1, Z_3 and Z_4 near the boundaries of domains 1 (AI), 2 (FH + CH + CI + FI + FRI) and 3 (ALH + ALI + MNI).

partially overlap or be disjoint. These random fields are modeled via the conventional multigaussian approach, as per the following steps:

(1) Cell declustering, using a common cell size of 200 m × 200 m × 10 m for all the variables. This size (approximately twice larger than the drill hole sampling

Table 10
Statistics before and after declustering.

Variable	Domain	Rock types	Mean value before declustering	Mean value after declustering
Z_2	1	MNI	0.0419	0.0443
Z_2	2	FH + CH + ALH + ALI + CI + FI + FRI + AI	0.0014	0.0018
Z_5	1	CI + FI	0.3724	0.4060

mesh) is selected to remove or, at least, to mitigate the effect of any possible preferential sampling. The largest relative changes in mean values before and after declustering are indicated in Table 10.

(2) Normal scores transformation and modeling of the declustered distributions of Z_1 to Z_6 through their Gaussian transformation functions within each domain.

(3) Inference of the spatial correlation structure, through the calculation of experimental covariances (22 direct covariances and 231 cross covariances). Here, the covariance is preferred to the variogram because the variables are not known at the same data locations (the domains in which they are defined may be disjoint), which prevents calculating cross-variograms (Wackernagel, 2003). The same calculation parameters as for the rock type indicators are used: lag separation distances multiple of 50 meters along the horizontal plane, and multiple of 10 meters along the vertical direction.

(4) Fitting of a linear coregionalization model, using a nugget effect and a set of nested exponential models. The coregionalization matrices are fitted with an automated procedure that aims at minimizing the squared differences between the experimental and modeled covariances (Goulard and Voltz, 1992; Emery, 2010). Note that a full coregionalization model is considered here, i.e., each of the 22 underlying Gaussian random fields is likely to be cross-correlated with any other, even if these random fields are defined on partially overlapping or on non-overlapping domains. Such a model allows accounting for spatial correlations between the variables of interest across the domain boundaries. Examples of experimental and fitted covariances are presented in Fig. 9. Although it captures the overall shape and correlation ranges of the experimental covariances, the fitting appears to be poorer than in the case of the rock type modeling shown in Fig. 5. This can be explained because of the reduced number of data available for each variable (the original data set is split into smaller subsets, each corresponding to a specific domain), making the experimental covariances more fluctuating, and because of the high number of covariances (253) that have to be fitted simultaneously with a single linear coregionalization model. Other fittings (not shown here) have been undertaken, but their impacts on the simulation results turn out to be marginal.

4.4. Joint simulation

The 22 Gaussian random fields are jointly simulated on the grid used for the simulation of rock types, via a spectral turning-bands algorithm (Emery et al., 2016). The conditioning to the drill hole data is realized by residual cokriging (Chilès and Delfiner, 2012), using up to 32 samples (192 normal scores data) located in an ellipsoid with semi-axes 250 m × 250 m × 100 m and centered at the target grid node. Twenty outcomes are constructed, each of which is associated with one outcome of the rock types. The simulated Gaussian values are back-transformed into the variables Z_1 to Z_6 (for each outcome and each target grid node, the back-transformation depends on the associated rock type outcome) and, subsequently, into the grades, loss on ignition and granulometry, as per Eq. (4). As an illustration, one outcome over a cross-section of the deposit is displayed in Fig. 10. This outcome gives one simulated value of each quantitative variable at each target grid node. The small-scale variability could be reduced by simulating on a fine grid and block-averaging the simulated values onto each block of size 10 m × 10 m × 10 m, as the change of support induces a spatial smoothing effect (Chilès and Delfiner, 2012).

4.5. Validation

A first validation consists of a visual check of the outcomes and their consistency with the rock type domains: each variable should exhibit spatial continuity within its geological domains, and discontinuities near the domain boundaries. This is particularly notorious in Fig. 10 with the iron and silica grades, when comparing hematite ores (iron rich, silica poor) and itabirites (iron poor, silica rich), and with the granulometry when comparing the friable and compact rock types.

A second validation consists in checking that the simulated values reproduce the marginal and bivariate distributions of the original drill hole data, which can be done by comparing the basic statistics, histograms, correlation coefficients and scatter diagrams, globally and/or within each rock type (Leuangthong et al., 2004); a few examples are shown in Table 11 and Fig. 11. By construction, the outcomes also perfectly reproduce the data values at the sampling locations and the stoichiometric closure formula linking the grades and the loss on ignition (Eq. (2)).

Finally, to verify the ability of the model to quantify the uncertainty at unsampled locations, leave-one-out cross-validation is performed on the drill hole data. At each data location, the grades, loss on ignition and granulometry are simulated conditionally to the information of the remaining data and rock types. From the outcomes so obtained, one can determine probability intervals on the true values for different theoretical probabilities and compare these probabilities with the proportions of data that belong to the intervals (Deutsch, 1997; Goovaerts, 2001). The results (Fig. 12) indicate a very good match for three elements (Fe, SiO_2 and Al_2O_3), with a deviation between the probabilities and data proportions always smaller than 4.3%, and a relatively good match for all the remaining elements, the greatest deviation being 8.4% for the 80 percent probability interval on granulometry (i.e., a relative error of only 10% on the nominal probability).

4.6. Post-processing

The outcomes allow quantifying the uncertainty in the recoverable resources, at the scale of the entire deposit or locally, on a block-by-block basis. A varied set of statistical tools and measures can be used to this end, such as: calculation of confidence limits and expected values for the grades, volumes and metal contents above given cut-offs; mapping of the probability of finding a given rock type or grades greater/lower than pre-specified cut-offs; definition of measures of variability over the outcomes for the entire deposit or specific blocks, etc. (Rossi and Deutsch, 2014 and references therein).

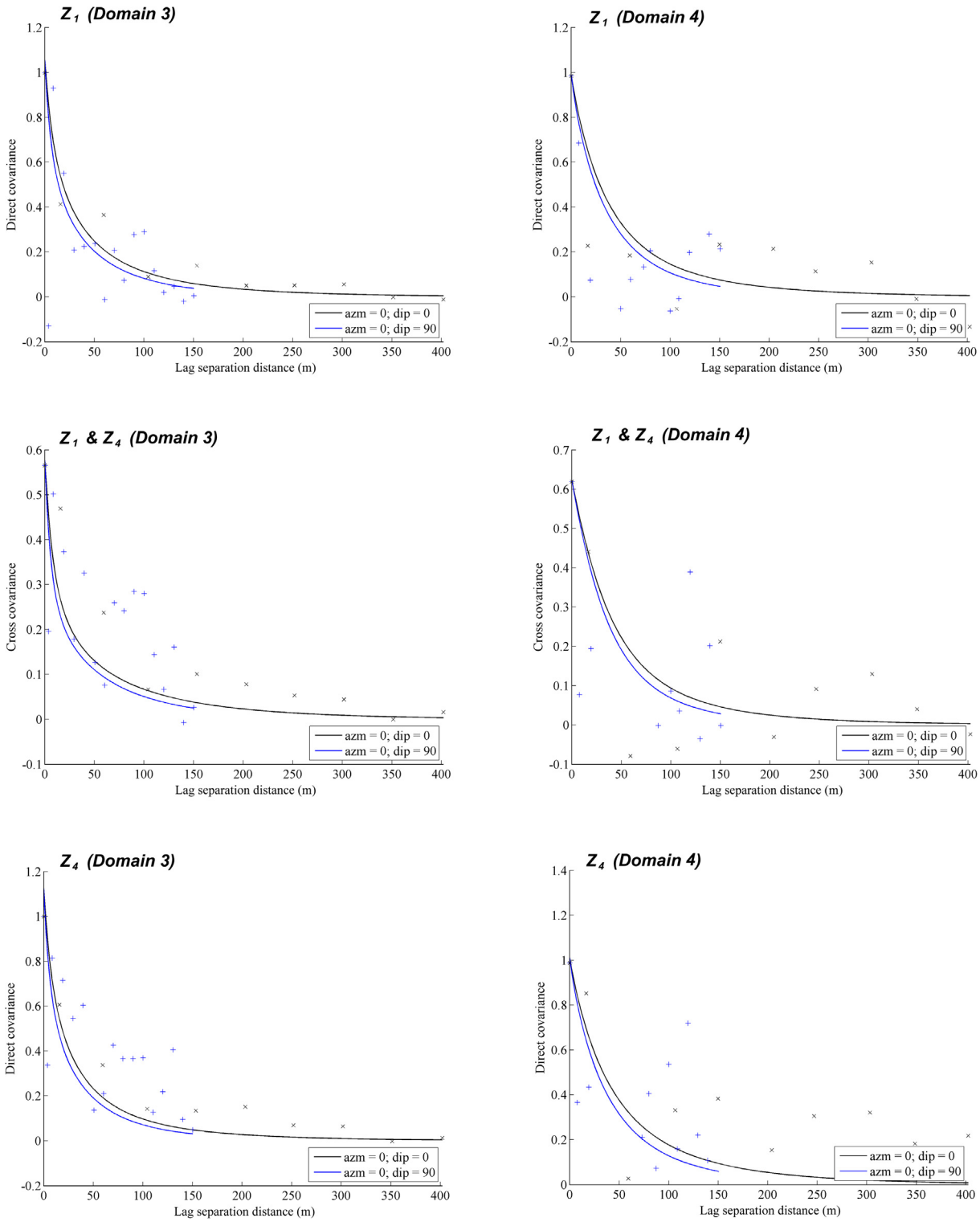

Fig. 9. Some examples of experimental (crosses) and fitted (solid lines) covariances, along the horizontal plane (black) and vertical direction (blue). (For interpretation of the references to colour in this figure legend, the reader is referred to the web version of this article.)

As a first example, Table 12 gives the fractions of volume and mean iron grades above cut-offs ranging from 40% to 55%, subject to maximum impurity grades: phosphorus less than 0.075% and alumina less than 2%. These figures have been calculated by considering each point as a minable unit and could be increased by blending material from different points. As a second example, Fig. 13 displays the mass proportions of hematite (Fe_2O_3), silicon dioxide (SiO_2), phosphorus pentoxide (P_2O_5), aluminum oxide (Al_2O_3), manganese monoxide (MnO) and loss on ignition (LOI) in each outcome, for the overall region and for specific blocks that have the same rock type over the 20 outcomes: manganese-rich itabirite (MNI), amphibolitic itabirite (AI) and canga (CG), respectively. The sum of the proportions is always equal to 100 because of the stoichiometric closure formula (Eq. (2)) but their values vary

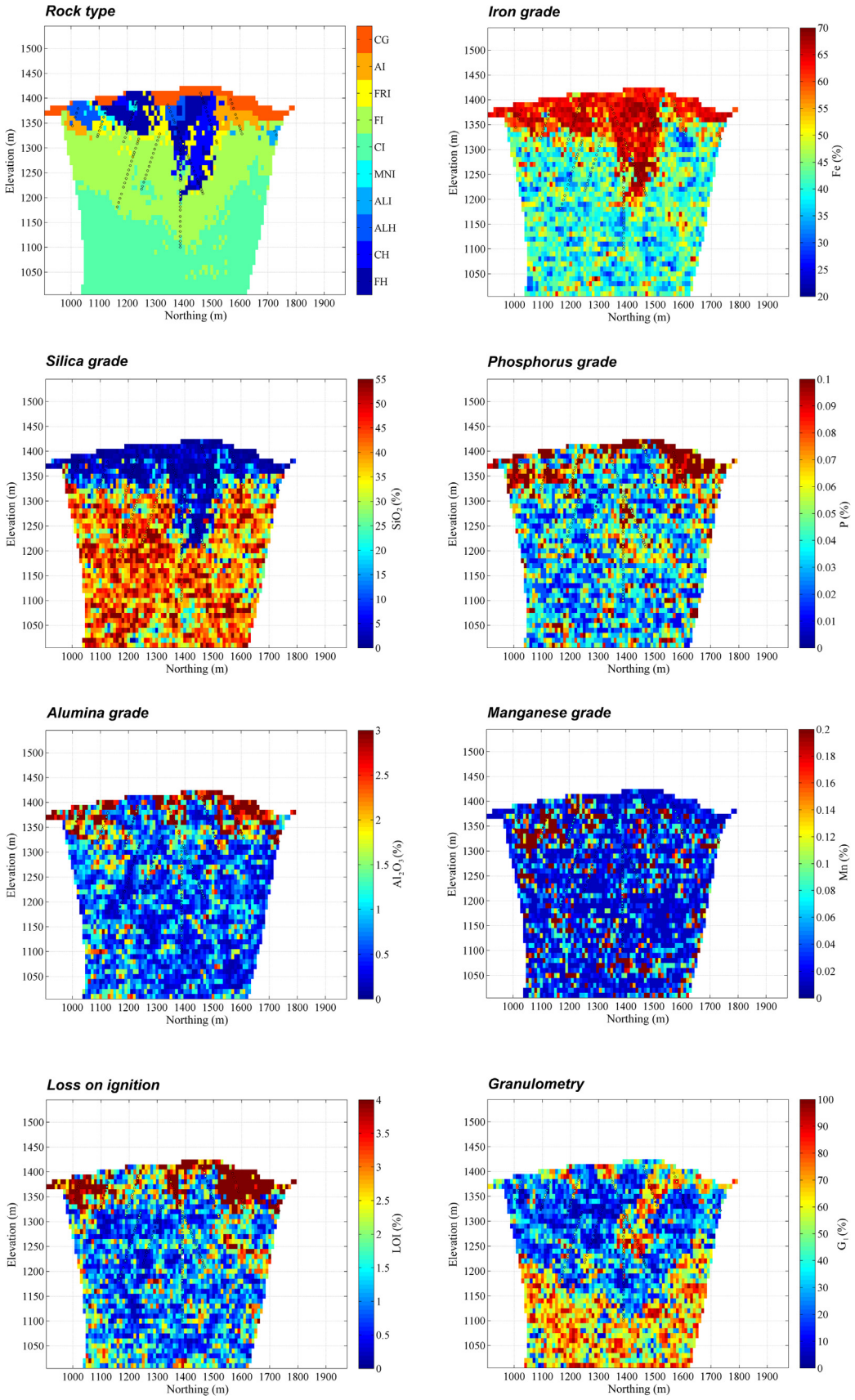

Fig. 10. Cross section of one outcome of the rock type, grades, loss on ignition and granulometry (easting = −6400 m).

Table 11
Minimum, maximum and average correlation coefficients on 20 simulated outcomes for specific pairs of variables and rock types.

First variable	Second variable	Rock types	Minimum correlation over 20 outcomes	Maximum correlation over 20 outcomes	Average correlation over 20 outcomes	Correlation observed on drill hole data
Fe	SiO_2	All	−0.99	−0.99	−0.99	−0.98
LOI	P	All	0.58	0.74	0.67	0.69
LOI	Al_2O_3	All	0.56	0.68	0.65	0.61
Fe	Al_2O_3	CG	−0.79	−0.68	−0.73	−0.80
Fe	LOI	CG	−0.77	−0.60	−0.72	−0.73

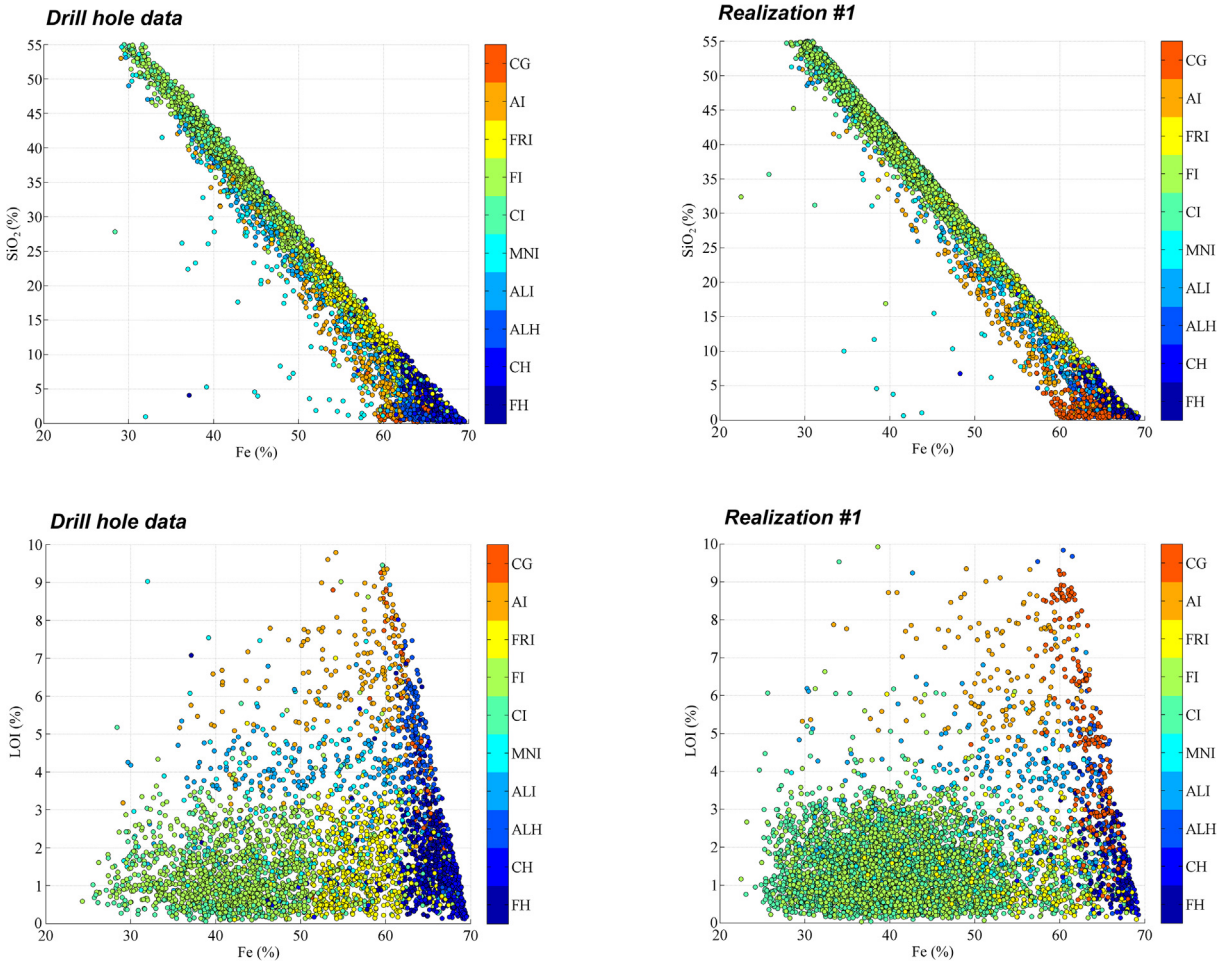

Fig. 11. Scatter diagrams of Fe vs. SiO_2 and Fe vs. LOI for drill hole data (left) and simulated values of first outcome (right).

considerably depending on the outcome and on the rock type. Due to the support effect (Chilès and Delfiner, 2012), the fluctuations in the proportions between one outcome and another are much smoother when considering the overall region (625,416 blocks) than when considering a single block.

5. Discussion and conclusions

The proposed plurigaussian model for simulating rock types allows reproducing (1) the contact relationships between rock type domains, (2) the local proportions of these domains (as inferred from the interpreted lithological model), (3) their spatial continuity, and (4) the observed data at the drill hole locations. The key is the use of a multidimensional truncation rule and efficient algorithms for Gibbs sampling and simulation. Few other geostatistical approaches can claim for such a versatility. For instance, sequential indicator simulation (Alabert, 1987) fails at imposing contact relationships, which may lead to compact hematite (high iron grade and coarse granulometry) being in contact with friable itabirite (low iron grade and fine granulometry), a situation that is avoided with the truncation rule defined in Fig. 4B. Alternatively, simulation based on multiple-point statistics (Mariethoz and Caers, 2014) could reproduce the desired contact relationships, but their implementation would be jeopardized by the lack of a representative training image of the rock type layout and by the non-stationarity of their spatial distribution (recall the discussion in Section 3.2).

Also, the simulation of the grades, loss on ignition and granulometry was not exempt from difficulties, starting with their mutual dependence relationships (as witnessed by their cross-correlations and the stoichiometric closure formula), as well as their complex dependence relationships with the rock types, corroborated by the geological domaining proposed in Section 4.2. Reproducing these relationships requires a versatile model (here,

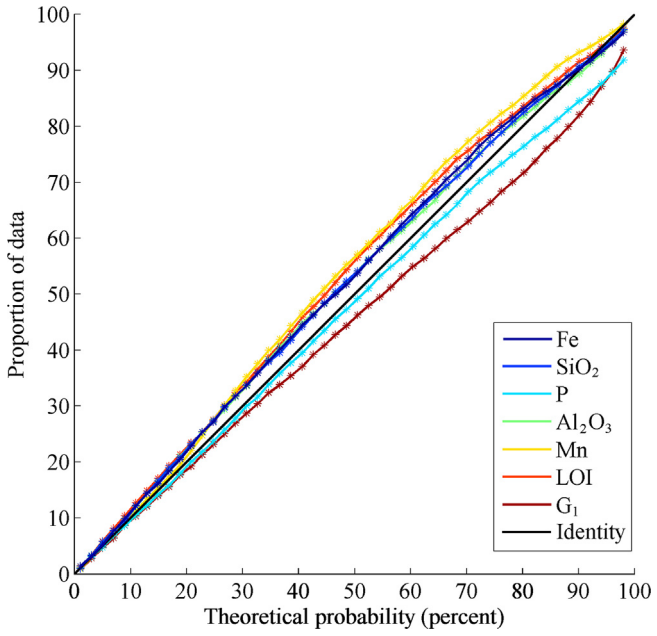

Fig. 12. Results of cross-validation for the simulation of quantitative variables.

multigaussian) and an efficient multivariate simulation algorithm (spectral turning-bands), without which the construction of outcomes would have been impractical. Some alternative algorithms could have been used, e.g., factorization via principal component analysis (Wackernagel, 2003), independent component analysis (Tercan and Sohrabian, 2013), minimum/maximum autocorrelation factors (Boucher and Dimitrakopoulos, 2009; Rondon, 2012) or coregionalization analysis (Wackernagel, 2003; Emery and Ortiz, 2012; Emery and Peláez, 2012), at the price of simplifications in the coregionalization modeling and difficulties in handling heterotopic data (although cross-correlated, the variables are not defined on the same domains). In contrast, because of the high number of variables (22) and their heterotopic design, simulation techniques based on cascaded simulation (Almeida and Journel, 1994), stepwise conditional transformations (Leuangthong and Deutsch, 2003) or super-secondary variables (Babak and Deutsch, 2009; Boisvert et al., 2013) would not be applicable here. Beyond this diversity of simulation algorithms, to the authors' knowledge, no practical alternative to the multigaussian model exists for such a highly multivariate simulation problem.

As a conclusion, the problem set in this paper was quite challenging, as it involved the joint modeling of coregionalized variables of different natures (nominal and quantitative) linked by complex dependence relationships. The proposed hierarchical

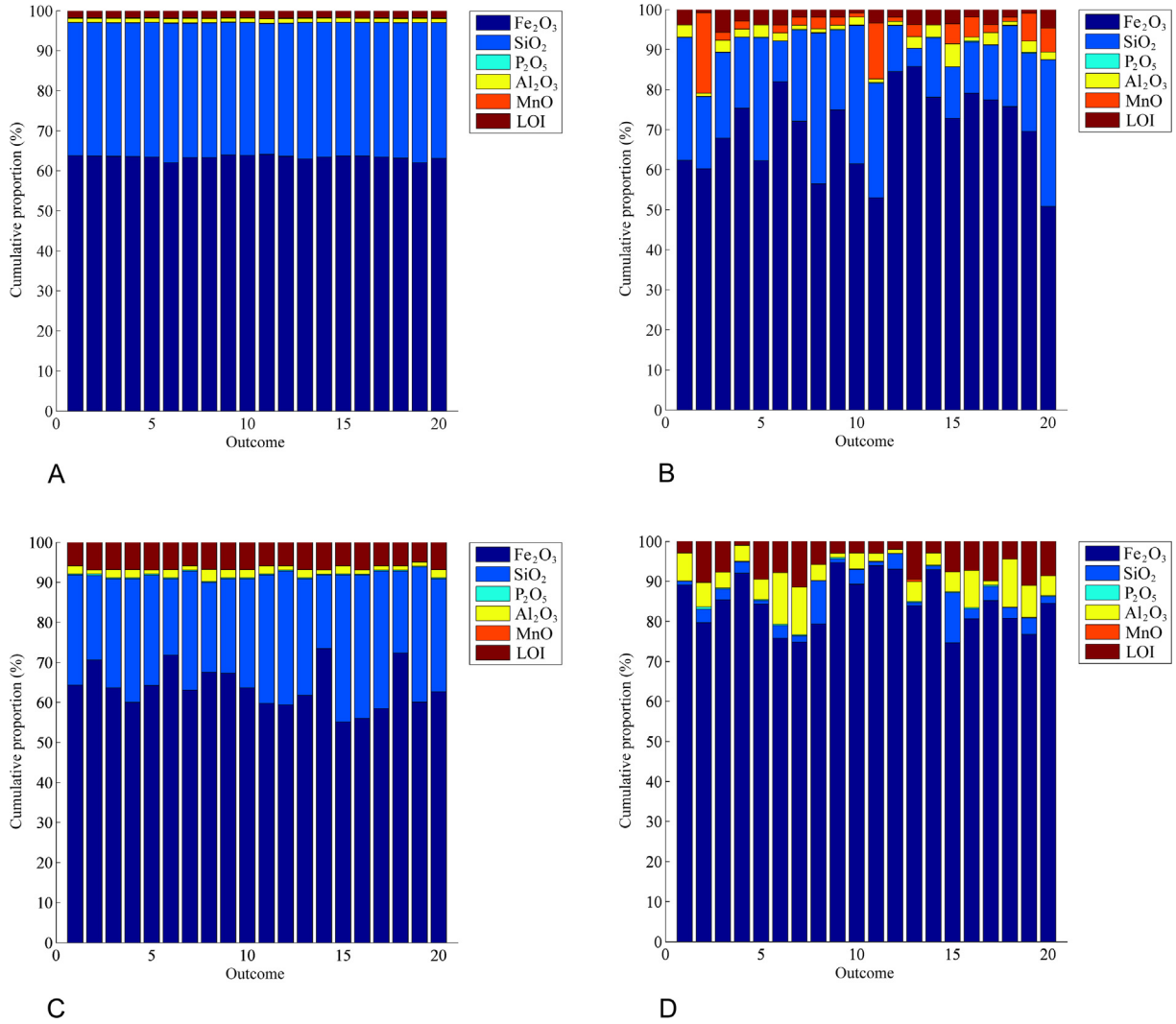

Fig. 13. Stoichiometric closure for (A) the overall ore region, (B) a block always simulated as manganese-rich itabirite (MNI), (C) a block always simulated as amphibolitic itabirite (IA), and (D) a block always simulated as canga (CG).

Table 12
Expected values and confidence limits for recoverable iron resources subject to P < 0.075% and Al_2O_3 < 2%

Iron cut-off grade (% Fe)	Fraction of volume			Mean iron grade (%)		
	Minimum over 20 outcomes	Maximum over 20 outcomes	Average over 20 outcomes	Minimum over 20 outcomes	Maximum over 20 outcomes	Average over 20 outcomes
40	0.421	0.460	0.445	48.6	49.1	48.8
45	0.250	0.267	0.259	53.2	53.6	53.3
50	0.131	0.141	0.136	58.6	58.9	58.7
55	0.085	0.091	0.088	62.3	62.4	62.4

approach successfully solved this problem, based on a combination of the plurigaussian and multigaussian models that offers unmatched flexibility, and on the choice of efficient simulation algorithms to address the numerical difficulties posed by the high number of variables, data and locations targeted for simulation. Of particular interest is the suggested geological domaining, which implies that a variable can evolve continuously across a rock type boundary, while another variable may be discontinuous when crossing the same boundary, although spatial cross-correlations do not vanish between both sides of this boundary. From a purely geological point of view, this feature makes sense as the geological controls are not the same for all the variables. For example, the iron and silica grades mainly depend on whether the prevailing rock type is hematite or itabirite, while the granulometry depends on whether the prevailing rock type is compact or friable.

Further research topics include the possibility to cross-correlate the Gaussian random fields $Y_1, \ldots, Y_6$ used in plurigaussian modeling, or to cross-correlate these random fields with the ones used to simulate the quantitative variables $(Z_1, \ldots, Z_6)$. Change-of-support models could also be investigated, as in the proposed approach the outcomes have to be constructed on a point support because $Z_1, \ldots, Z_6$ are not additive. Alternatively, change of support can be performed by simulating on a fine discretization grid and then averaging the simulated variables over each block.

Acknowledgments

This work was supported by VALE S.A., through the project entitled "Geostatistical cosimulation of grades and rock types for iron resource evaluation", by the COPEC-UC Foundation, through project 2014.J.057, and by the Chilean Commission for Scientific and Technological Research, through Project CONICYT PIA Anillo ACT1407.

References

Alabert, F., 1987. Stochastic imaging of spatial distributions using hard and soft information (Unpublished M.Sc. dissertation). Stanford University.
Almeida, A.S., Journel, A.G., 1994. Joint simulation of multiple variables with a Markov-type coregionalization model. Math. Geol. 26 (5), 565–588.
Armstrong, M., Galli, A., Beucher, H., Le Loc'h, G., Renard, D., Doligez, B., Eschard, R., Geffroy, F., 2011. Plurigaussian Simulations in Geosciences. Springer, Berlin.
Babak, O., Deutsch, C.V., 2009. Collocated cokriging based on merged secondary attributes. Math. Geosci. 41 (8), 921–926.
Beucher, H., Galli, A., Le Loc'h, G., Ravenne, C., 1993. Including a regional trend in reservoir modeling using the truncated Gaussian method. In: Soares, A. (Ed.), Geostatistics Tróia' 92. Kluwer, Dordrecht, pp. 555–566.
Boisvert, J.B., Rossi, M.E., Ehrig, K., Deutsch, C.V., 2013. Geometallurgical modeling at Olympic Dam mine, South Australia. Math. Geosci. 45 (8), 901–925.
Boucher, A., Dimitrakopoulos, R., 2009. Block simulation of multiple correlated variables. Math. Geosci. 41 (2), 215–237.
Chilès, J.P., Delfiner, P., 2012. Geostatistics: Modeling Spatial Uncertainty. Wiley, New York.
Deutsch, C.V., 1997. Direct assessment of local accuracy and precision. In: Baafi, E.Y., Schofield, N.A. (Eds.), Geostatistics Wollongong' 96. Kluwer, Dordrecht, pp. 115–125.
Dorr, J.V.N., 1964. Supergene iron ores of Minas Gerais, Brazil. Econ. Geol. 59 (7), 1203–1240.
Emery, X., 2007. Simulation of geological domains using the plurigaussian model: new developments and computer programs. Comput. Geosci. 33 (9), 1189–1201.
Emery, X., 2010. Iterative algorithms for fitting a linear model of coregionalization. Comput. Geosci. 36 (9), 1150–1160.
Emery, X., Ortiz, J.M., 2012. Enhanced coregionalization analysis for simulating vector Gaussian random fields. Comput. Geosci. 42, 126–135.
Emery, X., Peláez, M., 2012. Reducing the number of orthogonal factors in linear coregionalization modeling. Comput. Geosci. 46, 149–156.
Emery, X., Arroyo, D., Peláez, M., 2014. Simulating large Gaussian random vectors subject to inequality constraints by Gibbs sampling. Math. Geosci. 46 (3), 265–283.
Emery, X., Arroyo, D., Porcu, E., 2016. An improved spectral turning-bands algorithm for simulating stationary vector Gaussian random fields. Stoch. Env. Res. Risk Assess. 30 (7), 1863–1873.
Freulon, X., 1994. Conditional simulation of a Gaussian random vector with nonlinear and/or noisy observations. In: Armstrong, M., Dowd, P.A. (Eds.), Geostatistical Simulations. Kluwer, Dordrecht, pp. 57–71.
Goovaerts, P., 2001. Geostatistical modelling of uncertainty in soil science. Geoderma 103 (1–2), 3–26.
Goulard, M., Voltz, M., 1992. Linear coregionalization model: tools for estimation and choice of cross-variogram matrix. Math. Geol. 24 (3), 269–286.
Jones, P., Douglas, I., Jewbali, A., 2013. Modeling combined geological and grade uncertainty: application of multiple-point simulation at the Apensu gold deposit, Ghana. Math. Geosci. 45 (8), 949–965.
Kyriakidis, P.C., Deutsch, C.V., Grant, M.L., 1999. Calculation of the normal scores variogram used for truncated Gaussian lithofacies simulation: theory and FORTRAN code. Comput. Geosci. 25 (2), 161–169.
Le Loc'h, G., Galli, A., 1997. Truncated plurigaussian method: theoretical and practical points of view. In: Baafi, E.Y., Schofield, N.A. (Eds.), Geostatistics Wollongong' 96. Kluwer, Dordrecht, pp. 211–222.
Leuangthong, O., Deutsch, C.V., 2003. Stepwise conditional transformation for simulation of multiple variables. Math. Geol. 35 (2), 155–173.
Leuangthong, O., McLennan, J.A., Deutsch, C.V., 2004. Minimum acceptance criteria for geostatistical realizations. Nat. Resour. Res. 13 (3), 131–141.
Maleki, M., Emery, X., 2015. Joint simulation of grade and rock type in a stratabound copper deposit. Math. Geosci. 47, 471–495.
Maleki, M., Emery, X., Cáceres, A., Ribeiro, D., Cunha, E., 2016. Quantifying the uncertainty in the spatial layout of rock type domains in an iron ore deposit. Comput. Geosci. 20 (5), 1013–1028.
Mariethoz, G., Caers, J., 2014. Multiple-Point Geostatistics: Stochastic Modeling With Training Images. Wiley, New York.
Roldão, D., Ribeiro, D., Cunha, E., Noronha, R., Madsen, A., Masetti, L., 2012. Combined use of lithological and grade simulations for risk analysis in iron ore, Brazil. In: Abrahamsen, P., Hauge, R., Kolbjørnsen, O. (Eds.), Geostatistics Oslo 2012. Springer, Berlin, pp. 423–434.
Rondon, O., 2012. Teaching aid: minimum/maximum autocorrelation factors for joint simulation of attributes. Math. Geosci. 44 (4), 469–504.
Rossi, M.E., Deutsch, C.V., 2014. Mineral Resource Estimation. Springer, Dordrecht.
Talebi, H., Sabeti, E.H., Azadi, M., Emery, X., 2016. Risk quantification with combined use of lithological and grade simulations: application to a porphyry copper deposit. Ore Geol. Rev. 75, 42–51.
Tercan, A.E., Sohrabian, B., 2013. Multivariate geostatistical simulation of coal quality data by independent components. Int. J. Coal Geol. 112, 53–66.
Wackernagel, H., 2003. Multivariate Geostatistics: An Introduction With Applications. Springer, Berlin.
Yunsel, T.Y., Ersoy, A., 2011. Geological modeling of gold deposit based on grade domaining using plurigaussian simulation technique. Nat. Resour. Res. 20 (4), 231–249.